EPR Spectroscopy of Cu(I)−NO Adsorption Complexes Formed over Cu−ZSM-5 and Cu−MCM-22 Zeolites

V. Umamaheswari,[†] Martin Hartmann,[‡] and Andreas Pöppl*,[†]

Faculty of Physics and Geoscience, University of Leipzig, D-04103 Leipzig, Germany, and Department of Chemistry, Chemical Technology, University of Kaiserslautern, D-67653 Kaiserslautern, Germany

Received: July 13, 2004; In Final Form: September 28, 2004

The Cu(I)−NO adsorption complexes were formed over copper exchanged and autoreduced high siliceous Cu−ZSM-5 and Cu−MCM-22 zeolites and studied by EPR spectroscopy at X-, Q-, and W-band frequencies. The spin Hamiltonian parameters of the Cu(I)−NO species are indicative of a nitrogen-centered radical complex with a bent geometry and a significant contribution of the Cu(I) 4s atomic orbital to the wave function of the unpaired electron. Two different Cu(I)−NO species were found in both zeolites. It has been confirmed by comparing the experimental data with the results of previous theoretical studies that the presence of two different species is due to the formation of Cu(I)−NO adsorption complexes from two different Cu(I) sites in the zeolite matrix with different numbers of oxygen coligands. The structure of the two sites in the Cu−ZSM-5 and Cu−MCM-22 zeolites must be similar as the spin Hamiltonian parameters are found to be almost independent of the zeolite matrix, where the Cu(I)−NO complex is formed. The EPR signal intensity of the Cu(I)−NO species was studied as a function of the NO loading, and the formation of diamagnetic Cu(I)−$(NO)_2$ species with rising NO pressure at the expense of paramagnetic Cu(I)−NO monomers could be demonstrated for both systems at low temperatures.

1. Introduction

Nitrogen oxides (NOx) are hazardous pollutants formed as byproducts during the combustion processes in industrial boilers and vehicle engines and are responsible for smog formation, acid rain, and global warming.[1] Many metal ion exchanged zeolites have been reported to be active for catalytic decompostion[2] and reduction of nitrogen monoxide,[3] indicating the great affinity of the NO molecule for the zeolites. Among many metal ion exchanged zeolites, copper catalysts have received much attention due to their activity and selectivity toward the decomposition of these nitrogen oxides (NOx). The catalytic decomposition of NO is the simplest and most desirable method for the removal of NO from exhaust streams, and Cu−zeolites are the most suitable catalysts for the reaction among the many catalysts reported.[4,5] Especially high siliceous zeolites such as ZSM-5 and MCM-22 have been reported to be promising catalysts for the NO decomposition process.[6,7] Low siliceous zeolites are less active, due to their inability to stabilize reaction intermediates that may be required for further transformations. Although the fundamental reason why the low siliceous zeolites are less active is not yet understood completely, it has been reported that low siliceous zeolites such as Y zeolite release their excess oxygen, following an oxidation treatment, more easily than the more active high siliceous zeolites such as Cu−ZSM-5 zeolite.[8] Hence clarification of the state of the NO adsorbed, the interaction of NO with Cu(I), and the reaction mechanism are remarkably important for the progress in the chemistry of NO decomposition and design of decomposition catalysts. The Cu(I)−NO complexes are some of the most important intermediates in the decomposition processes. The interaction of NO with Cu(I) is reported to be a complex redox process where the oxidation of the site is proposed to occur via the elimination of N_2O from dinitrosyl through the formation of Cu(I)−$(NO)_2$ from monomeric Cu(I)−NO complexes.[9]

Several spectroscopic studies, such as electron paramagnetic resonance (EPR), infrared (IR) spectroscopy, and extended X-ray absorption fine structure spectroscopy (EXAFS), aiming at the structure of the Cu(I)−NO complexes over many Cu exchanged zeolites such as Cu−Y, Cu−L, Cu−ZSM-5, and Cu−MCM-22 have been reported.[10−16] Both mononitrosylic Cu(I)−(NO) and dinitrosylic Cu(I)−$(NO)_2$ complexes have been identified by IR spectroscopy.[7] However, the detailed structure of these complexes is largely unknown. EPR spectroscopy is especially useful because it provides direct access to the determination of the electronic and geometric structures of the adsorption complexes, as well as the sites where the Cu(I)−NO species are formed in the zeolites, which are essential for the proper understanding of the catalytic activity of the zeolitic materials, as recently shown for Cu(I)−NO in Cu−ZSM-5 zeolites.[15] Most catalytic, spectroscopic, and theoretical studies of nitric oxide in copper exchanged zeolites have been focused on the ZSM-5[17−20] system because of its great potential for the NO decomposition process even at higher temperatures such as 773 K.

Typically the Cu(I) form of the zeolite is obtained by autoreduction of Cu(II) exchanged zeolites, which is achieved by thermal treatment under high vacuum, and this process involves simple dehydration between two adjacent hydroxy forms of Cu(II) species present in the ion exchange sites of the zeolite.[21] Two Cu(II) species are observed in the EPR spectra of copper exchanged ZSM-5 zeolites, which have been assigned to Cu(II) in square planar and square pyramidal configurations.[22] Broclawik et al.[23] have reported that after reduction the Cu(I) moves through the zeolite matrix to finally occupy cation

* Corresponding author. E-mail: poeppl@physik.uni-leipzig.de.
[†] University of Leipzig.
[‡] University of Kaiserslautern.

10.1021/jp046907r CCC: $30.25
Published on Web 01/07/2005

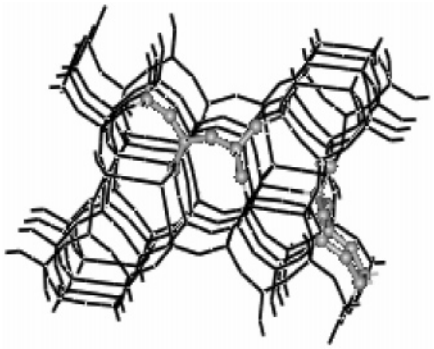

Figure 1. Location of M7 and I2 sites in the ZSM-5 framework. The M7 site is located in the wall of the main channel, and the I2 site is in the intersection of the main and zigzag channels.

positions where the number of coordinated framework oxygen atoms (O_f) is less compared to the initial Cu(II) cation sites. An average oxygen coordination number of 2−3 was predicted for Cu(I) cations in ZSM-5 on the basis of EXAFS experiments.[24]

Zeolite ZSM-5 has a three-dimensional structure[25] defined by 10-membered-ring openings. The straight or main channels parallel to [010] (5.6 × 5.3 Å) intersect at right angles with the sinusoidal channels along [100] (5.1 × 5.5 Å). The walls of these channel system offer a large variety of potential sites to host the Cu(I) cations. Recently, two different Cu(I) cationic sites, namely M7 and I2 (Figure 1), have been identified by quantum chemical calculations in Cu−ZSM-5 zeolites as the potential NO adsorption sites.[26,27] The M7 sites located at the main channel comprise two joint five-membered rings, where three out of seven T atoms are common and can therefore be considered to be a more robust version of the simpler five-membered centers. In the M7 site the Cu(I) ion, proposed to be located in the vicinity of the Al atom, is highly confined to only one of the twin five-membered rings. According to Pietrzyk et al.[27] the Cu(I) in this site exhibits asymmetric trigonal coordination with two longer (d_{Cu-O} = 2.025 Å and d_{Cu-O} = 2.047 Å) Cu−O bonds and one shorter (d_{Cu-O} = 1.980 Å) Cu−O bond. The distinctly smaller I2 site protruding into the intersection of the main and sinusoidal channels consists of a central AlO_4 surrounded by two SiO_4 tetrahedra terminated by OH groups. In the I2 site the Cu(I) is coordinated only to two oxygen atoms of the AlO_4 tetrahedron in the framework with comparable Cu−O bond lengths (d_{Cu-O} = 1.951 Å and d_{Cu-O} = 1.954 Å).[27] Slightly different Cu−O bond lengths have been reported by Nachtigallova et al.[26] for the two Cu(I) cation sites.

In addition to Cu−ZSM-5 zeolites, Cu−MCM-22 zeolites have also been reported as potential catalysts for the NO decomposition. MCM-22, a recently synthesized (IZA code MWW) medium-pore high silica zeolite, possesses interesting structural and physicochemical properties.[28] Its structure contains two noninterconnected channel systems both accessed by 10-membered-ring (MR) windows: a 10-MR sinusoidal two-dimensional channel system (4.0 × 5.5 Å), similar to that of the zigzag channels in ZSM-5, and a 12-MR system formed by interconnected supercages (7.1 × 7.1 × 18.2 Å). Similar to zeolite Cu−ZSM-5, Wasowicz et al.[29] have observed two different Cu(II) species A and B by EPR and assigned those two species to the Cu(II) cations present in two different ion exchange sites in the MCM-22 matrix, namely (1) the major species A arising from Cu(II) in either type II or IV sites located in front of the five-ring in a large interlayer supercage and intralayer two-dimensional sinusoidal channel, respectively, and (2) the minor species B from type III sites (in front of the planar six-ring, hexagonal prism window, in a large interlayer supercage). Although the location of Cu(II) in the MCM-22 matrix is clearly defined, the exact location of Cu(I), which is formed after reduction of Cu(II) in MCM-22, is not yet known. However, it is possible to identify sites similar to those of I2 and M7 as observed in ZSM-5 framework in the large cage structure of the MCM-22 framework, as shown in Figure 2. The site similar to I2 could be identified in the 12-MR system formed by interconnected supercages, and the site similar to M5 could be identified in front of the five-ring in a large interlayer supercage and intralayer two-dimensional sinusoidal channel, which is also identified by EPR as the location of major Cu(II) species A. Frache et al.[7] have reported the presence of two different Cu(I) and Cu(II) sites in Cu exchanged MCM-22 samples after vacuum treatment at 823 K by IR studies of adsorbed CO and NO probes. In contrast to Cu−ZSM-5 zeolite, the IR studies[7] also confirm the presence of two different Cu(I)−NO species in Cu−MCM-22 loaded with NO. In addition to that, the oxidation of Cu(I)−NO to Cu(II) at high NO adsorption pressure, at room temperature, is reported to be rapid, suggesting that this catalyst is also a potential candidate for the NO decomposition reaction. We have already reported the formation of Cu(I)−NO complexes in Cu−MCM-22 zeolites through EPR,[30] and although the presence of two different Cu(I)−NO species is also confirmed, the exact location of the different Cu(I) ions in the MCM-22 zeolite matrix, which is responsible for the formation of these species, is still unknown.

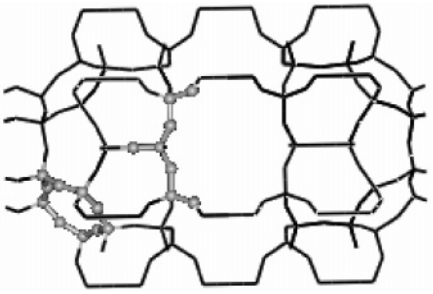

Figure 2. Unit cell structure of the MCM-22 framework showing two possible Cu(I) cationic sites.

In the present study we have investigated the formation of Cu(I)−NO complexes over Cu−ZSM-5 and Cu−MCM-22 by EPR spectroscopy at various frequencies (X-, Q-, and W-bands). The increased spectral resolution and separation of the Cu(I)−NO signals from the Cu(II) signal at higher frequencies (Q- and W-bands) allows a reliable determination of the spin Hamiltonian parameters from the EPR powder patterns which in turn yields a detailed characterization of the formed adsorption complexes. A comparison with the results of recently published quantum chemical calculations of Cu(I)−NO moieties allows us to identify the Cu(I) cation sites where NO is adsorbed. In addition, we have also studied the dependence of Cu(I)−NO and Cu(II) EPR signal intensities on the NO pressure. This will provide additional information about the formation of monomeric Cu(I)−NO, dimeric Cu(I)−$(NO)_2$, and Cu(II)−NO intermediates in these potential catalysts.

2. Experimental Section

Sample Preparation. ZSM-5 (Si/Al = 17) was synthesized according to the already reported procedure,[31] and the following gel composition was used: SiO_2:0.03Al_2O_3:1.97NH_4OH:0.10TPABr:31.48H_2O. In a typical synthesis 3 g of $Al(NO_3)_3$ and 4.6 g of tetrapropylammonium bromide were dissolved in 32 g of water. To this mixture 32 g of Ludox AS 40 (40%

SiO_2) and 43.6 g ammonium hydroxide were added to form the gel and stirred well. The gel was then transferred into a stainless steel autoclave, and the hydrothermal synthesis was carried out at 453 K under rotation (50 rotations per minute) for 5 days. The contents were then cooled and transferred to 1000 mL of demineralized water and heated to 338 K. The obtained solid was then filtered and washed thoroughly with water and dried in an oven at 373 K. The as-synthesized material was finally calcined in air at 813 K for 18 h.

MCM-22 (Si/Al = 22) was synthesized using the procedure reported by Unverricht et al.,[32] and the following gel composition was used: SiO_2:0.02Al_2O_3:0.5HMI:0.6NaOH:41.2H_2O:0.17H_2SO_4. In a typical synthesis, 50.7 g of Cab-osil M5 (Fluka) (30% silica) was added to NaOH (6 g) and hexamethyleneimine (Aldrich) (HMI) (12.4 g) mixture and stirred. The resultant mixture was added to 3.5 g of $Al_2(SO_4)_3$·18H_2O in 87.5 g of water. Then 4.5 g of H_2SO_4 was added dropwise and stirred. The resultant mixture was transferred to an autoclave and crystallized at 423 K for 4 days under rotation. The material was then filtered, dried, and calcined at 773 K for 12 h under N_2 and air flow. The calcined materials were characterized by powder X-ray diffraction. The ammonium form of the materials was obtained by liquid-state ion exchange of the calcined materials with NH_4NO_3, and the obtained solids were then ion exchanged with $Cu(CH_3COO)_2$. The extent of copper exchange was found to be 66% for Cu−ZSM-5 and 88% for Cu−MCM-22. Prior to the adsorption of NO, the samples were activated at 673 K under vacuum ($p < 1 \times 10^{-7}$ Pa) in a 100% steel vacuum line (to prevent NO from reacting with small amounts of residual oxygen) for 14 h. Subsequently, the samples were cooled to 300 K and 5 Pa of NO was introduced for the X- and Q-band samples and 0.5 Pa was used for the W-band samples. Taking into account different geometries for X-, Q-, and W-band samples and attached valves, this procedure ensured having approximately 1 NO molecule adsorbed per 40 unit cells for all three samples. Thereafter, the samples were cooled to liquid nitrogen temperature and sealed off.

Spectroscopic Measurements. The EPR spectra were recorded at X-band ESP 380 (n_{mw} = 9.4 GHz), Q-band EMX 10−40 (n_{mw} = 33.9 GHz), and W-band E680 (n_{mw} = 94.2 GHz) Bruker spectrometers at temperatures of 77 K (X-band) and 10 K (Q- and W-bands). The magnetic flux density B_0 of the magnet coils used for X- and Q-band EPR was calibrated by the ^{1}H NMR magnetometer MJ110R. A LiF standard with g_{LiF} = 2.002 288 (4) was used for the B_0 calibration of the cryomagnet (W-band). The B_0 modulation amplitudes used were 0.7 mT (X-band) and 0.2 mT (Q-band), and the modulation frequencies were adjusted to n_{mod} = 100 kHz at X- and W-bands and 70 kHz at Q-band. The microwave power used was low enough to prevent saturation of the spin systems. For X-, Q-, and W-band measurements EPR quartz tubes with outer diameter of about 3.8, 1.8, and 0.8 mm, respectively, were used. The NO pressure dependence of the Cu(I)−NO (formed over Cu−MCM-22 and Cu−ZSM-5) EPR signal intensity was studied at the X-band at 77 K at various NO pressures ranging from 1 to 220 Pa. Each time the same amount (0.01 g) of fresh copper exchanged zeolite sample was subjected to the sample treatment described above and then the desired amount of NO was introduced. A DPPH sample was used as intensity standard in a TE_{104} two-sample cavity for the EPR measurements.

3. Results

Multifrequency EPR of Cu(I)−NO Complexes. Figures 3 and 4 show the X-, Q-, and W-band EPR spectra of Cu−ZSM-5 and Cu−MCM-22 after activation at 400 °C in a vacuum and subsequent NO adsorption at 300 K. Although autoreduction of Cu(II) to Cu(I) takes place to a large extent, the signal of Cu(II) is still clearly visible. At X-band frequencies (Figures 3a and 4a), the Cu(II) signal is superimposed by the intense spectra of the Cu(I)−NO complexes and, therefore, an exact

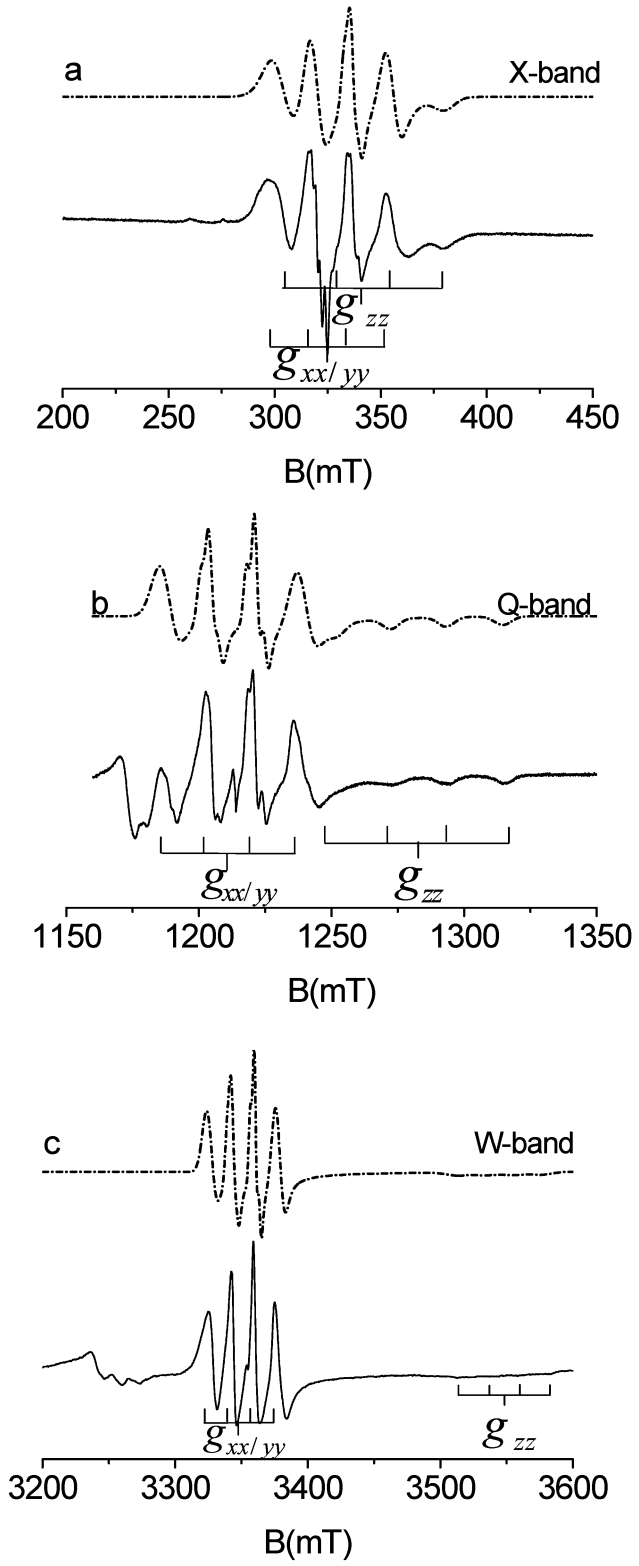

Figure 3. Experimental (—) and simulated (···) (a) X-, (b) Q-, and (c) W-band EPR spectra of Cu(I)−NO species formed over Cu−ZSM-5 zeolite, adsorbed at NO pressures of 5 (X-, Q-bands) and 0.5 Pa (W-band). The stick diagrams indicate the Cu hf splitting of the Cu(I)−NO EPR signal at the $g_{xx/yy}$ and g_{zz} spectral regions.

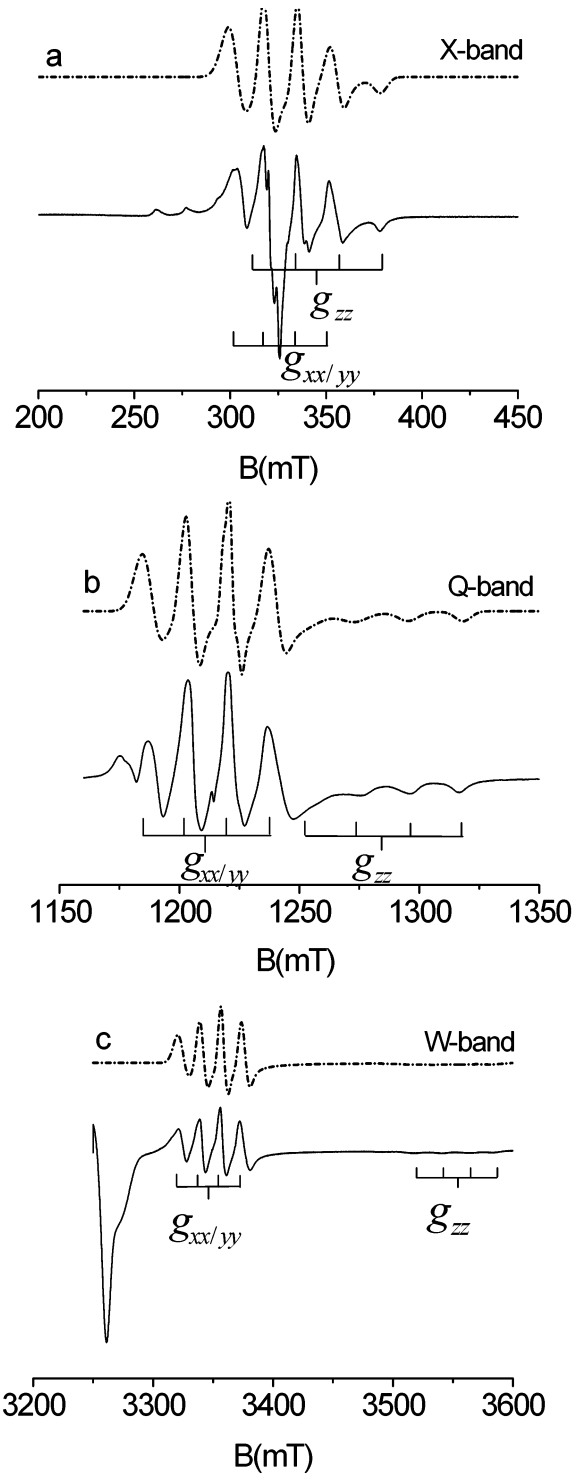

Figure 4. Experimental (—) and simulated (···) (a) X-, (b) Q-, and (c) W-band EPR spectra of Cu(I)−NO formed over Cu−MCM-22, adsorbed at NO pressures of 5 (X-, Q-bands) and 0.5 Pa (W-band). The stick diagrams indicate the Cu hf splitting of the Cu(I)−NO EPR signal at the $g_{xx/yy}$ and g_{zz} spectral regions.

determination of the spin Hamiltonian parameters of these complexes is impossible. In the Q-band spectrum (Figures 3b and 4b), the Cu(II) signal is almost separated from that of the Cu(I)−NO complexes. Finally, at the W-band frequency, complete separation between the Cu(II) signal and the signals of the Cu(I)−NO complexes is achieved (Figures 3c and 4c). The Cu(I)−NO complexes formed from both systems (Cu−ZSM-5 and Cu−MCM-22) show an anisotropic spectrum, where the ^{63}Cu ($I = 3/2$) hyperfine (hf) splitting into four lines is clearly visible in the g_{zz} and $g_{xx/yy}$ spectral regions. For the Cu−MCM-22 sample an additional triplet splitting of about 3 mT is observed in the $g_{xx/yy}$ spectral region, because of ^{14}N ($I = 1$) hf interaction with the central nitrogen nucleus of the NO molecule. In samples with lower NO loadings the nitrogen hf triplet splitting approaches an intensity ratio of 1:3:1, which is found to be characteristic for NO adsorption complexes with metal ion surface sites.[33−36] In the case of Cu−ZSM-5 the ^{14}N hf triplet in the Q-band EPR spectra of Cu(I)−NO complexes is not resolved at NO pressure of 5 Pa but could be observed at lower NO pressures of about 0.5 Pa (see Figure S1 in Supporting Information) corresponding to approximately 1 NO molecule per 400 unit cells.[16] It seems to be natural to assume that progressive line broadening effects due to magnetic dipole−dipole interactions among the formed Cu(I)−NO adsorption complexes lead to a smearing of the ^{14}N hf triplet with increasing NO pressures. We have to note that the ^{14}N hf splitting could not be resolved in the g_{zz} spectral region of the EPR powder pattern of the Cu(I)−NO complexes. The observed copper hf interaction evidences the formation of the NO adsorption complex with the Cu(I) cation,[15,16] where a substantial delocalization of the unpaired spin density in the Cu(I) atomic orbitals (AOs) occurs. However, the ^{14}N hf coupling of about 3 mT resolved in the $g_{xx/yy}$ spectral region and the fact that $g_{zz} < g_{xx/yy}$ indicate that the major part of the wave function of the unpaired electron is still centered at the NO molecule.

The spin Hamiltonian parameters of the Cu(I)−NO complexes formed in both systems (Cu−ZSM-5 and Cu−MCM-22) have been determined by simulation of the experimental EPR powder patterns using the Easyspin EPR simulation package[37] and are summarized in Table 1.

The simulation of the powder spectra are based on the following spin Hamiltonian:

$$\hat{H} = \beta_e \boldsymbol{B}\mathbf{g}\hat{\boldsymbol{S}} + \hat{\boldsymbol{S}}\mathbf{A}^{Cu}\hat{\boldsymbol{I}}^{Cu} + \hat{\boldsymbol{S}}\mathbf{A}^{N}\hat{\boldsymbol{I}}^{N} \qquad (1)$$

where the first term with the tensor **g** describes the electron Zeeman interaction. The other two terms take into account the copper and nitrogen hf interactions measured by the tensors $\mathbf{A}^{Cu}$ and $\mathbf{A}^{N}$. All other symbols have their usual meaning. The hyperfine interactions of both ^{63}Cu (natural abundance 69.1%) and ^{65}Cu (natural abundance 30.9%) isotopes having nuclear spin $I = 3/2$ have been included in the simulation procedure, but presented coupling constants will always refer to the ^{63}Cu isotope throughout the paper.

According to standard convention the principal axis system of the tensors **g** and $\mathbf{A}^{N}$ are defined in such a way that their *z*-axis points along the N−O bond and the *y*-axis defines the symmetry axis of the NO Π_y^* molecular orbital (MO) where the unpaired electron resides (Figure 5).[34] Since NO is a p-type radical, the g_{xx} and g_{yy} principal axes can be readily distinguished in its EPR spectrum by the ^{14}N hf triplet splitting of about 3 mT along the *y*-axis. The Euler angles α, β, and γ give the transformation between **g** or $\mathbf{A}^{N}$ tensor principal axis frame and the principal axis frame of the Cu hf interaction tensor $\mathbf{A}^{Cu}$. Simulations were done simultaneously for X-, Q-, and W-band spectra in an iterative procedure so that the multifrequency EPR experiments could be evaluated by a single parameter set.

A comparison of the X-, Q- and W-band EPR spectra in Figures 3 and 4 indicates that the **g** tensor of the Cu(I)−NO complexes is axially symmetric within the experimental error of $|g_{xx} - g_{yy}| = \pm 0.0002$. The frequency-dependent line broadening at the g_{zz} spectral region arises from a distribution $\delta g_{zz} = 0.01$ in the principal value g_{zz} as reported earlier.[16,33] The overall intensity pattern at the $g_{xx/yy}$ region of the Cu hf

TABLE 1: Spin Hamiltonian Parameters and Covalent Parameter *l* of Cu(I)−NO Complexes Formed over Cu−ZSM-5 and Cu−MCM-22 Zeolites

Cu(I)−NO system	Cu−ZSM-5 (species A)	Cu−ZSM-5 (species B)	Cu−MCM-22 (species A)	Cu−MCM-22 (species B)
$g_{xx/yy}$	2.0050	2.0050	2.0043	2.0043
g_{zz}	1.8900	1.8999	1.8952	1.8980
δg_{zz}	0.01	0.01	0.01	0.01
A^{N}_{yy} (10^{-4} cm^{-1})	29	29	33	33
A^{Cu}_{xx} (10^{-4} cm^{-1})	158	158	157	157
A^{Cu}_{yy} (10^{-4} cm^{-1})	130	130	133	133
A^{Cu}_{zz} (10^{-4} cm^{-1})	216	239	200	220
A^{Cu}_{iso} (10^{-4} cm^{-1})	168	175	163	170
α (deg)	90	90	90	90
β (deg)	35	35	35	35
γ (deg)	90	90	90	90
l	0.85	0.78	0.81	0.79

quartet of the EPR powder spectrum of the Cu(I)−NO complexes suggests that the **g** and $\mathbf{A}^{Cu}$ tensors are not collinear. Simulations of the powder spectra show that the intensity pattern especially at the $g_{xx/yy}$ region is very sensitive with respect to the selection of the Euler angles. Furthermore, the characteristic intensity pattern of the nitrogen hf triplet at $g_{xx/yy}$ indicates that the Cu hf splitting along g_{xx} and g_{yy} axes must be comparable because $g_{xx} \approx g_{yy}$; hence, an orthorhombic tensor $\mathbf{A}^{Cu}$ is expected in the case of noncollinear principal axis frames of **g** and $\mathbf{A}^{Cu}$. The Euler angles obtained for these two systems, $\alpha = 90°$, $\beta = 35°$, and $\gamma = 90°$, show that the principal axis system of the tensor $\mathbf{A}^{Cu}$ is rotated about the common g_{xx}/A^{Cu}_{xx} axes by an angle $\beta = 35°$ versus the **g** tensor frame, where the A^{Cu}_{zz} principal axis lies within the *yz*-plane of the **g** and nitrogen hf coupling tensor principal axis system (Figure 5). Alternative sets of Euler angles, such as $\alpha = 0$, $\beta = 35°$, $\gamma = 0$, corresponding to rotation about common g_{xx}/A^{Cu}_{yy} axes, do not give satisfactory agreement with experimental spectra and hence can be ruled out. The spin Hamiltonian parameters evaluated by the spectral simulations of the Cu(I)−NO complex (species A) formed over Cu−ZSM-5 and Cu−MCM-22 are summarized in Table 1. The isotropic Cu hf interaction parameter A^{Cu}_{iso} calculated by $A^{Cu}_{iso} = (1/3)\ \mathrm{Tr}(\mathbf{A}^{Cu})$ is likewise presented in Table 1. We note that only A^{N}_{yy} could be evaluated from the ^{14}N hf triplet splitting at $g_{xx/yy}$. The other principal values $A^{N}_{xx/zz}$ of the tensor $\mathbf{A}^{N}$ cannot be determined by the continuous-wave EPR experiments since the N hf splitting is not resolved.

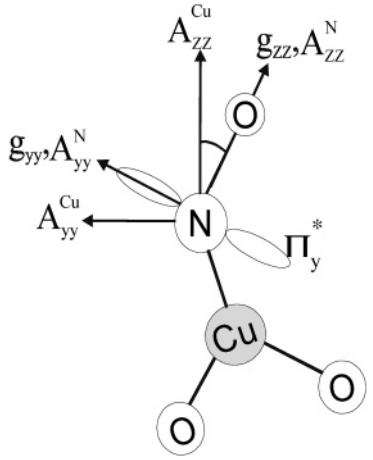

Figure 5. Orientation of principal axes frames of the tensors **g**, $\mathbf{A}^{N}$, and $\mathbf{A}^{Cu}$ of the Cu(I)−NO moiety. The $\mathbf{A}^{Cu}$ frame is rotated by the Euler angle β about the common *x* principal axis, but the A^{Cu}_{zz} principal axis is not necessarily parallel to the Cu−N bond. The *yz* plane of the **g** tensor is spanned by the N−O bond and the symmetry axis of the Π^{*}_{y} MO of the NO molecule.

Analysis of the line broadening at the g_{xx} and g_{zz} spectral regions including *g* strain just provided upper limits $A^{N}_{xx/zz} < 1.1 \times 10^{-4}$ cm^{-1} for these principal values.

A close inspection of the g_{zz} spectral region in the Q-band EPR spectra of Cu(I)−NO complexes formed over Cu−ZSM-5 and Cu−MCM-22 zeolites reveals the formation of a minor species B in addition to the presence of the major species A for both materials, as illustrated in Figure 6. Obviously species A and B differ in their g_{zz} and A^{Cu}_{zz} parameters (Table 1). However, no additional spectral features due to the minor species B have been observed at the $g_{xx/yy}$ region and hence the other spin Hamiltonian parameters must be assumed to those of species A within the given experimental errors.

NO Pressure Dependence. In addition to the multifrequency EPR studies of the Cu(I)−NO complex, the influence of the NO loading pressure in the sample preparation on the formation of Cu(I)−NO and possible Cu(II)−NO complexes was studied at X-band frequencies. We note that the situation for Cu(I)−NO and Cu(II)−NO is somewhat complementary. The Cu(I)−NO adsorption complex is accessible by EPR and the Cu(I) adsorption site is EPR silent, whereas the reverse situation holds for the adsorption of nitric oxide at Cu(II) cations. Figure 7 shows the X-band EPR spectra of NO adsorbed samples at various NO pressures in comparison with the dehydrated material prior to NO adsorption, for both Cu−ZSM-5 and Cu−MCM-22 zeolites, respectively. It can be inferred from the spectra that the Cu(I)−NO signal intensity is appreciable at moderate NO pressure but it diminishes with further increase in NO pressure; finally at a certain maximum NO pressure the

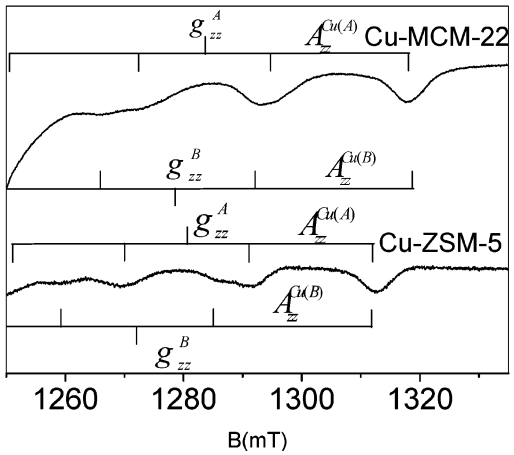

Figure 6. Q-band spectra of Cu(I)−NO complexes in Cu−ZSM-5 and Cu−MCM-22 showing two species A and B in the g_{zz} spectral region. The stick diagrams indicate the Cu hf splitting of the Cu(I)−NO EPR signals of species A and B at the g_{zz} spectral region.

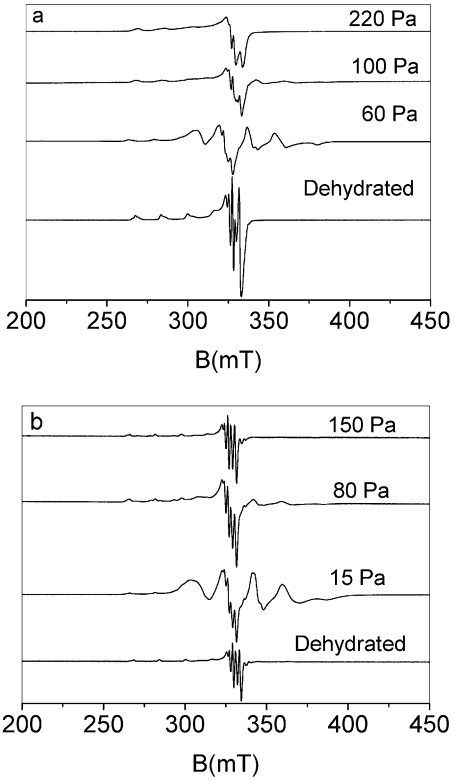

Figure 7. X-band spectra (at 77 K) of Cu(I)−NO complexes formed over (a) Cu−ZSM-5 and (b) Cu−MCM-22 at different NO adsorption pressures.

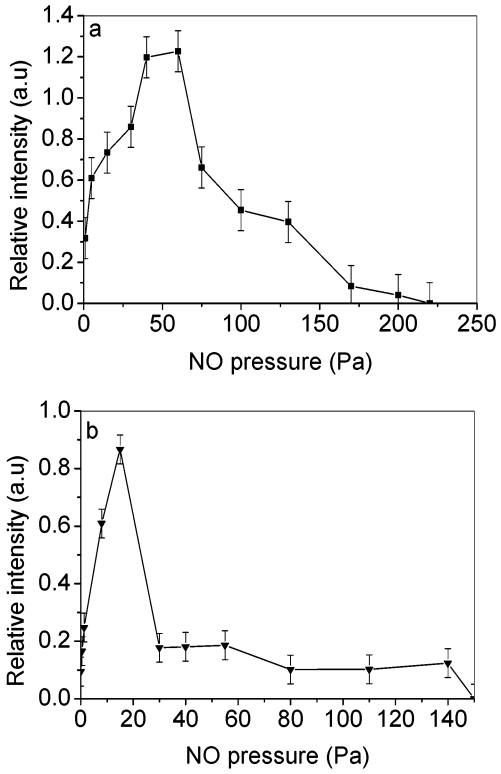

Figure 8. NO pressure dependence of the relative intensity at 77 K of the Cu(I)−NO EPR signal in (a) Cu−ZSM-5 and (b) Cu−MCM-22 zeolites measured at the X-band.

Cu(I)−NO signal vanishes completely and only the Cu(II) signal is observed. The relative intensities of the Cu(I)−NO EPR signals as a measure of the concentration of the adsorption complex as a function of the NO pressure were determined at 77 K and are illustrated in parts a and b of Figure 8for Cu−ZSM-5 and Cu−MCM-22, respectively. Since the EPR spectra of the Cu(I)−NO species heavily overlaps with that of the Cu-(II) cations, a double integration was not feasible and the Cu-(I)−NO signal intensity was determined by taking the amplitude of the undisturbed Cu hf line at 360 mT with respect to the standard DPPH sample. This approach is justified since no (Cu−MCM-22) or only moderate (Cu−ZSM-5) line broadening of the Cu(I)−NO EPR signal was observed due to NO adsorption. In the case of the Cu−ZSM-5 system the Cu(I)−NO signal intensity increases with increasing NO adsorption pressure and attains a maximum at about 50 Pa; then it decreases rapidly and reaches zero at 220 Pa. In the case of Cu−MCM-22 system, the maximum intensity could be observed at a lower NO pressure of approximately 15 Pa; then the intensity decreases rapidly and reaches zero at a comparably lower pressure of 150 Pa.

To check if the formation of one of the Cu(I)−NO complex species A or B is preferred, Q-band spectra of Cu−ZSM-5 and Cu−MCM-22 materials after adsorption at 0.5 and 5.0 Pa NO pressures were recorded at 10 K. Figure 9 illustrates the g_{zz} spectral region of the obtained spectra. It is obvious that the NO adsorption pressure does not have any influence on the intensity ratio between the signals of species A and B for Cu−ZSM-5 (Figure 9a) within the experimental error of about 20%. Otherwise, for Cu−MCM-22 zeolites (Figure 9b), only species A is formed at low NO pressures (0.5 Pa). The formation of species B occurs at elevated NO pressures of approximately 5 Pa and higher. No significant dependence of the spin Hamiltonian parameters of the Cu(I)−NO complexes on the NO adsorption pressure have been observed for both materials.

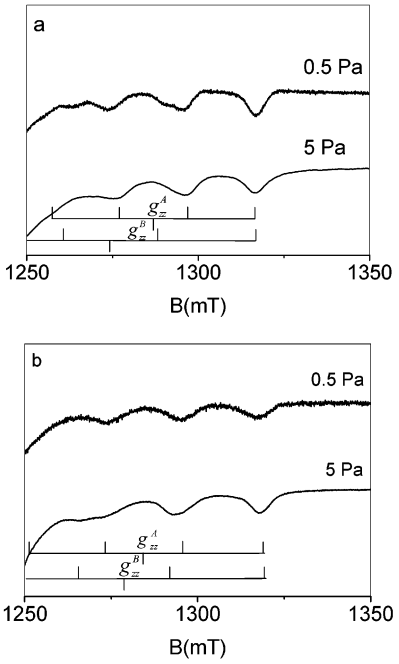

Figure 9. NO pressure dependence of the g_{zz} spectral region in Q-band spectra of Cu(I)−NO species A and B at 10 K: (a) Cu−ZSM-5; (b) Cu−MCM-22. The stick diagrams indicate the Cu hf splitting of the Cu(I)−NO EPR signals of species A and B at the g_{zz} spectral region.

The influence of NO adsorption pressure on the intensity and the spin Hamiltonian parameters of the Cu(II) species was also studied for both Cu−ZSM-5 and Cu−MCM-22. Two different Cu(II) cation species could be detected on the basis of the X-band EPR data in the dehydrated materials in accordance with

TABLE 2: Spin Hamiltonian Parameters of Cu(I) Cations in Dehydrated Cu−ZSM-5 and Cu−MCM-22 Zeolites and after NO Adsorption at 220 Pa (Cu−ZSM-5) and 150 Pa (Cu−MCM-22)

catalyst	$g_\perp$	$g_{\|\|}$(species A)	$g_{\|\|}$(species B)	$A^{Cu}_{\|\|}$(species A) (10^{-4} cm^{-1})	$A^{Cu}_{\|\|}$(species B) (10^{-4} cm^{-1})
Cu−ZSM-5 (dehydrated)	2.043	2.318	2.302	172	175
Cu−ZSM-5 (220 Pa of NO)	2.044	2.324	2.295	171	179
Cu−MCM-22 (dehydrated)	2.047	2.331	2.322	171	181
Cu−MCM-22 (150 Pa of NO)	2.047	2.329	2.322	171	179

earlier results.[13,29] Their **g** tensor and Cu hf coupling parameters measured for the dehydrated materials and after adsorption of NO at pressures of 220 (Cu−ZSM-5) and 150 Pa (Cu−MCM-22) are summarized and given in Table 2. Again no change in the spin Hamiltonian parameters upon NO adsorption has been observed. However, we note that the EPR spectra of the Cu(II) cations in Cu−ZSM-5 materials indicate a significant line broadening with increasing NO loadings as seen in Figure 7a. Such line broadening effects in the Cu(II) EPR spectra are absent for zeolite Cu−MCM-22 (Figure 7b). The Cu(II) EPR signal intensity as a measure of the relative cupric ion concentration in both the dehydrated and the NO adsorbed samples (NO pressures 220 and 150 Pa for Cu−ZSM-5 and Cu−MCM-22, respectively) were determined by double integration of the corresponding EPR signal with respect to the standard DPPH sample. It has been found that the intensities before and after adsorption do not differ significantly. Hence the relative Cu(II) cation concentration is not influenced by NO adsorption within the experimental error limit of 20% and we can rule out the formation of EPR silent Cu(II)−NO complexes at the expense of the paramagnetic Cu(II) cation species under the used experimental conditions.

4. Discussion

Electronic Structure of the Cu(I)−NO Complex. The observed ^{14}N hf coupling and the relation of the **g** tensor principal values $g_{zz} < g_{xx/yy}$ for the Cu(I)−NO species (see Table 1) is indicative for nitric oxide adsorption complexes with a dominating p-type radical character.[33,34] However, the large copper hf splitting evidences a substantial delocalization of the unpaired spin density in the 3d and 4s Cu(I) AOs which leads to significant differences in the **g** tensor and metal ion hf coupling parameters of the Cu(I)−NO species in comparison with NO adsorption complexes with first and second main group metal ions.

In the latter case, the **g** tensor principal values can be evaluated in terms of an electrostatic interaction model according to[35,38]

$$g_{xx} = g_e\frac{\Delta}{\sqrt{\lambda^2+\Delta^2}} - \frac{\lambda}{E}\left(\frac{\Delta-\lambda}{\sqrt{\lambda^2+\Delta^2}} - 1\right)$$

$$g_{yy} = g_e\frac{\Delta}{\sqrt{\lambda^2+\Delta^2}} - \frac{\lambda}{E}\left(\frac{\Delta-\lambda}{\sqrt{\lambda^2+\Delta^2}} + 1\right)$$

$$g_{zz} = g_e - \frac{2l\lambda}{\sqrt{\lambda^2+\Delta^2}} \qquad (2)$$

Here g_e is the free electron g value, $\lambda = 123$ cm^{-1} is the NO spin−orbit coupling constant,[39] and Δ and E are the energy splitting between the NO $^2\Pi^*$paramagnetic ground state and the $^2\Pi^*$and $^2\Sigma^*$ excited electronic states, respectively. The quantity l has the meaning of a covalency factor and measures the effective g factor of the orbital contribution.[38] This phenomenological parameter equals 1 for free NO or purely ionic bonding schemes and offers the opportunity to correct the g_{zz} principal value for possible spin delocalization ($l < 1$). Equation 2 provides the relation $g_{zz} < g_{xx/yy} < g_e$ and has been successfully used to interpret the **g** tensor of Na(I)−NO adsorption complexes formed over Na−A and Na−ZSM-5 zeolites,[33] where the NO−metal ion bond is strongly ionic.[40] In contrast, the **g** tensor principal values of the Cu(I)−NO complexes formed over the Cu−ZSM-5 and Cu−MCM-22 zeolites (Table 1) follow the order $g_{zz} < g_e < g_{xx/yy}$, which indicates contributions of copper 3d AOs to the singly occupied molecular orbital (SOMO)[16] due to an appreciable covalent nature of the Cu(I)−NO bond. Indeed, Neyman et al.[41] recently reported that the covalent character of the Cu(I)−NO bond contributes significantly to the **g** tensor anisotropy of Cu(I)−NO complexes. On the basis of quantum chemical calculations the contribution of the 3d AOs of Cu to the SOMO of NO was found to be the sole reason for the deviations of the **g** tensor principal values from those predicted by eq 2, and the experimentally obtained relation $g_{zz} < g_e < g_{xx/yy}$ could be verified for isolated Cu(I)−NO moieties. Although eq 2 fails to predict the proper order of the g tensor components in the case of Cu(I)−NO species, it can be used to determine their covalency parameter l (Table 1) as a rough estimate for the spin delocalization in the adsorption complexes. The parameters l were determined from the g_{zz} principal values by using eq 2 and $\Delta = 0.272$ eV [33] taken from the experimentally obtained parameters of Na(I)−NO complexes in Na−ZSM-5. The values of $l \approx 0.8$ suggest that about 80% of the spin density is localized in the NO Π^*_yMO and approximately 20% is shared between the Cu(I) AOs and the Σ MO of NO with the major part at the copper ion, a value in reasonable agreement with previous experimental results[15] and theoretical predictions.[27,42]

In principle, more detailed information on the geometric and electronic structures of the Cu(I)−NO moiety can be deduced from the copper hf coupling tensor $\mathbf{A}^{Cu}$. The orientation of the principal axis frame of $\mathbf{A}^{Cu}$ with respect to the tensors **g** and $\mathbf{A}^N$ as defined by the Euler angles in Table 1 suggests a bent complex geometry, where the Cu−N bond is within a plane spanned by the N−O bond and the symmetry axis of Π^*_yMO of the adsorbed NO molecule (Figure 5). Such a bent complex geometry with C_S symmetry allows overlap of Cu(I) 4s, $3d_{z^2}$, $3d_{yz}$ AOs with the electron spin bearing Π^*_yMO of the nitric oxide molecule. The admixture of Cu(I) AOs to the SOMO explains qualitatively the large metal ion hf coupling which is quite exceptional for NO adsorption complexes.

Recently, considerable theoretical efforts have been undertaken to interpret quantitatively the Cu hf coupling of Cu(I)−NO complexes. Sojka et al.[15] applied the MO−LCAO approach where the SOMO with the unpaired electron was derived on the basis of the C_S complex symmetry:

$$|\Phi_{SOMO}\rangle = b_1|\Pi^*_y\rangle + b_2|\Sigma\rangle + c_1|3d_{z^2}\rangle + c_2|3d_{yz}\rangle + c_3|4s\rangle \qquad (3)$$

The contribution of the 4s (c_3) and 3d (c_1, c_2) copper AOs to the SOMO were derived from the A^{Cu}_{iso} value and a partitioning of the components of the anisotropic Cu hf coupling tensor T^{Cu}_{ii}

$= A_{ii}^{Cu} - A_{iso}^{Cu}$, respectively. A Cu−N−O bond angle of $\alpha = 18°$ was then calculated from the coefficients c_1 and c_2 and the angle between the g_{zz} and A_{zz}^{Cu} principal axes. However, the application of this approach seems to be dubious in such cases of significant admixture of metal ion 3d AOs to the SOMO because these contributions may lead to considerable deviations of the **g** tensor *z*-axis from the N−O bond direction as reported by Neyman et al.[41] for isolated Cu(I)−NO moieties. Furthermore, spin polarization effects in the formally doubly occupied orbitals may significantly influence the spin-density distribution, leading to possible misinterpretation of the experimental results; therefore our results are just discussed in relation to previous quantum chemical calculations based on density functional theory (DFT).[27,42] The spin density at the individual atomic centers is determined by two effects: the coordinative spin transfer from NO to unoccupied valence orbitals of Cu(I) and the spin polarization in formally doubly occupied orbitals of the system. In a recent paper Freysoldt et al.[42] could demonstrate by DFT methods that both effects can yield large but opposing contributions to the anisotropic Cu hf coupling tensor $\mathbf{T}^{Cu}$ of Cu(I)−NO complexes. The A_{iso}^{Cu} value was found to be significantly less subjected to spin polarization processes. Therefore, we restrict ourselves to the interpretation of A_{iso}^{Cu} in the following discussion. The isotropic hf coupling is mainly determined by two parameters: the Cu−N−O bond angle and the charge transfer of coligands to the Cu(I), which prevents the spin transfer from the NO adsorbate molecule.[42] In general, A_{iso}^{Cu} decreases with increasing Cu−N−O bond angle α. A larger value of α reduces the spin transfer from NO to Cu(I) due to decrease in overlap between the spin bearing Π^* MO of the NO and the copper 4s AO. Furthermore, a continuous decrease in the parameter $A_{iso}^{Cu}$with increasing number of oxygen coligands could be established by DFT methods for a series of charged ($[(H_2O)_n(NO)Cu]^+$) and neutral ($[(H_2O)_{n-1}(OH)(NO)Cu]$) model complexes with increasing number *n* of water ligands.[42] For the isolated Cu(I)−NO complex A_{iso}^{Cu} was found to be between 400 and 600 $\times 10^{-4}$ cm^{-1}, which is much higher than the experimentally observed values for Cu(I)−NO species (Table 1). The best agreement between theoretical prediction and experimental A_{iso}^{Cu} values could be obtained for either a 2-fold (183×10^{-4} cm^{-1}) or a 3-fold (159×10^{-4} cm^{-1}) oxygen coordination. Taking into account the experimentally found relation A_{iso}^{Cu}(species A) < A_{iso}^{Cu}(species B) (Table 1), we tentatively assign the Cu(I)−NO species A and B to $(RO)_3$Cu(I)−NO and $(RO)_2$Cu(I)−NO moieties, respectively. The assignment is qualitatively supported by the order of the covalency factors of the two species, *l*(species A) > *l*(species B), derived from the corresponding g_{zz} values (Table 1), which indicate a larger transfer of unpaired electron spin density from the Π_y^* MO of the NO to the Cu(I) ion for species B.

Suggestions for Cu(I) Adsorption Sites. The natural assignment of the Cu(I)−NO species A and B to specific Cu(I) cation sites for the Cu−ZSM-5 system is that they are formed at the two suggested cation sites M7 and I2 (Figure 1). Previous DFT calculations by Pietrzyk et al.[27] support the assignment. Isotropic Cu hf couplings of 158.7×10^{-4} and 168.7×10^{-4} cm^{-1} for Cu(I)−NO complexes formed at M7 and I2 sites were reported, which are in close agreement with the experimental EPR results and predict the presence of two adsorption complexes with distinctly different A_{iso}^{Cu} values that in turn can be associated with these sites. In the DFT calculations the authors[27] used a simpler five-membered-ring cluster (M5(7)) to model the M7 site, but which retains its basic properties. In the case of Cu(I)−NO formed at the I2 site, the Cu(I) cation coordinates with two framework oxygen atoms with almost identical Cu−O bond lengths (1.971, 1.976 Å) and hence possess a larger A_{iso}^{Cu} value. NO complex formation at the M5(7) site changes the copper−oxygen coordination. The Cu(I) ion coordinates to two framework oxygens with Cu−O bond lengths of 1.991 and 2.056 Å, and the bond to the third previously bound oxygen considerably lengthens to 2.700 Å. Thus the number of oxygen coligands for the Cu(I)−NO complex formed at site M5(7) is not strictly defined and is about two to three but obviously results in a lower A_{iso}^{Cu} value in comparison with the well-defined 2-fold oxygen coordination of the I2 site. The calculated Cu−N−O bond angles were 148° (I2) and 151° (M5(7)). Hence we may conclude that the presence of two Cu(I)−NO species A and B with different A_{iso}^{Cu} and g_{zz} parameters can be explained by the formation of the Cu(I)−NO complexes at different cation sites, where the Cu(I) coordinates with either exactly two or two to three framework oxygens. This result is in agreement with the theoretically predicted decrease in A_{iso}^{Cu} with increasing number of oxygen coligands.[42] Hence it seems to be justified for Cu−ZSM-5 zeolites to assign species A and B with lower and higher isotropic copper hf couplings to Cu(I)−NO species formed at M5(7) and I2 sites, respectively.

The spin Hamiltonian parameters obtained for the Cu(I)−NO species A and B formed over the Cu−MCM-22 zeolites are similar to the results obtained for the Cu(I)−NO species formed over Cu−ZSM-5 zeolites (Table 1). Especially their A_{iso}^{Cu} parameters are only slightly smaller in comparison with the isotropic hf couplings found for Cu(I)−NO complexes formed at the M5(7) and I2 Cu(I) cation sites in Cu−ZSM-5. This indicates that the environment and location of the Cu(I) cations forming the Cu(I)−NO complexes in MCM-22 do not differ much from that of the M5(7) and I2 sites in the ZSM-5 framework structure. Hence, although the exact nature and location of Cu(I) in Cu−MCM-22 is not reported yet, it can be assumed from the experimental results that NO is adsorbed at cation sites in Cu−MCM-22 which are similar to these M5(7) and I2 sites known for ZSM-5 zeolites. Indeed, similar Cu(I) cation sites can be identified in the MCM-22 structure (Figure 2). Furthermore, we like to note that Davidova et al.[44] showed very recently that the structure and spectroscopic properties of the Cu(I)−NO complex are primarily determined by the local oxygen coordination of the Cu(I) cation after the formation of the adsorption complex rather than the zeolite framework structure. The slightly smaller A_{iso}^{Cu} values of species A and B in Cu−MCM-22 in comparison with the Cu−ZSM-5 system (see Table 1) may indicate that the different framework types lead to a small increase in the Cu−N−O bond angles of the Cu(I)−NO moieties in Cu−MCM-22. However, the deviations are small and we conclude that the difference in the structure of the zeolite matrix does not influence A_{iso}^{Cu} much, and it is only the number of framework oxygen coordination of Cu(I) and the resulting charge transfer from the framework oxygen coligands to the cation that determine the isotropic copper hf interaction in these systems. It is also found that the Si/Al ratio of the Cu−ZSM-5 and Cu−MCM-22 zeolites does not have any significant influence on the EPR parameters of the formed Cu(I)−NO complexes.[30] A comparison of the distribution widths δg_{zz} of the g_{zz} principal value of the **g** tensor between Cu(I)−NO ($\delta g_{zz} = 0.010$) and Na(I)−NO ($\delta g_{zz} = 0.029$) complexes for ZSM-5 zeolites[16,33] leads to the same conclusion: The host matrix has only a minor effect on the Cu(I)−NO moiety and its electronic structure seems to be almost solely determined by the oxygen coligands of the cation.

Influence of NO Pressure on the EPR Intensity of the Cu(I)−NO Complexes. The relative concentration of the Cu(I)−NO complexes formed over Cu−ZSM-5 as measured by their EPR signal intensity shows a characteristic dependence on the NO loading, as seen in Figure 8a. The Cu(I)−NO EPR signal intensity rises with increasing NO adsorption pressure, attains its maximum at around 50 Pa, and then it decreases rapidly at higher NO pressures and finally falls to zero at high NO pressures of about 220 Pa. The reason for the increase in Cu(I)−NO signal intensity with increase in NO pressure in the initial state is due to the increase in the Cu(I)−NO monomer formation. At first a single NO molecule is adsorbed at each Cu(I) cation present in the accessible sites resulting in the formation of Cu(I)−NO monomers; as more and more sites are getting involved in the complex formation, the Cu(I)−NO signal intensity increases. No preference for NO adsorption at either the M5(7) or I2 Cu(I) site could be observed as seen from the g_{zz} spectral region of the Q-band EPR spectra of species A and B taken at different NO loadings (Figure 9a). When the NO pressure is increased further, once all the Cu(I) sites are filled with monomers, EPR silent dimers, Cu(I)−$(NO)_2$, having a singlet ($S = 0$) ground state are formed. It is noteworthy that although a triplet ($S = 1$) ground state has been experimentally confirmed in the case of Na(I)−$(NO)_2$ adsoprtion complexes in Na−A zeolites,[36] a singlet ground state has been predicted by quantum chemical calculations[43] for NO dimer formation at Cu(I) cations. The dimers are formed because of the adsorption of a second molecule of NO on the EPR active monomeric Cu(I)−NO, which results in the decrease of the Cu(I)−NO signal intensity. At 220 Pa formation of the Cu(I)−NO signal is completely lost (Figure 8a) and dimer formation is completed. The monomer and dimers have been likewise found by IR[9,25] at low temperature and room temperature. Moreover, it is also confirmed by IR studies that the dimer is formed at the expense of Cu(I)−NO monomers which are formed at low NO adsorption pressures. IR studies[9] have further proven that, at higher NO pressure, Cu(II) and N_2O are formed because of the decomposition of the Cu(I)−$(NO)_2$ at room temperature. Hence Cu(I)−$(NO)_2$ has been confirmed as one of the essential intermediates during NO decomposition which occurs over dehydrated copper exchanged zeolites. Because oxidation of Cu(I) to Cu(II) by NO occurs instantaneously, only at room or higher temperatures, the formation of, for instance, Cu(II)−NO species is not reported at low temperatures over the dehydrated Cu−ZSM-5 zeolite through IR.[9] Since our studies have been carried out at low temperature (77 K), no such oxidation is expected in the present case. Indeed, the Cu(II) ESR signal intensity was observed to be the same for dehydrated samples and samples loaded at higher NO pressures (150 and 200 Pa) in accordance with the previous IR results.[9] The formation of Cu(II)−NO is reported to involve the transfer of the unpaired electron from the Π_y^* MO of the NO to the partially filled 3d AOs of the Cu(II) ion, resulting in the partial oxidation of NO and hence partial reduction of Cu(II).[9] Therefore, the Cu(II)−NO complex is EPR silent ($S = 0$) and its formation could not be checked through EPR directly, but of course is expected to result in a decrease of the Cu(II) EPR signal intensity. However, since there is no significant decrease in the Cu(II) EPR signal intensity when compared to the original dehydrated Cu(II) signal, the formation of the Cu(II)−NO complexes in our system at low temperatures can likewise be ruled out. The only noticeable effect of NO adsorption on the Cu(II) EPR spectrum is an obvious increase in its line width due to g and A strain at higher NO loading (Figure 7a). We assume that NO molecules, which are adsorbed in close proximity to the Cu(II) ions, slightly modify the Cu(II) spin Hamiltonian parameters and in that way cause a distribution in the principal values of the **g** and copper hf coupling tensors.

The overall characteristic of NO adsorption over Cu−MCM-22 zeolites is found to be comparable to Cu−ZSM-5 but displays also some distinct characteristic features. The Cu(I)−NO complexes formed in Cu−MCM-22 show NO pressure dependence (Figure 8b) similar to that of Cu−ZSM-5, but the Cu(I)−NO signal intensity maximum is already obtained at NO pressures of about 15 Pa and the Cu(I)−NO signal is completely lost at 150 Pa versus 220 Pa observed for the Cu−ZSM-5 system. This indicates that complete formation of EPR silent Cu(I)−$(NO)_2$ dimers occurs at lower NO loadings in Cu−MCM-22 in comparison with Cu−ZSM-5. The two adsorption steps, the filling of the Cu(I) adsorption sites initially by one NO molecule and subsequently by two NO molecules, with increasing NO loadings seem to be better separated from each other for the Cu−MCM-22 zeolite. The difference in behavior of Cu−MCM-22 compared to Cu−ZSM-5 may be attributed to the difference in the framework structure of the zeolite. The formation of Cu(I)−NO monomers at low NO adsorption pressure and Cu(I)−$(NO)_2$ dimers at high NO pressures has also been observed by IR spectroscopy at low temperature in Cu−MCM-22.[7] However, a direct comparison of the NO doses, where the interconversion of the monomer into the dimer species occurs, between the IR experiments reported by Frache at al.[7] and our work does not seem to be justified because the experiments were conducted in different ways. A further distinct difference of the Cu−ZSM-5 system is the preference of one Cu(I) adsorption site at low NO loadings. It is obvious from the Q-band spectra illustrated in Figure 9a that there is a significant change in the relative population of two Cu(I)−NO species A and B with increasing NO pressure. At 0.5 Pa, species A with the smaller A_{iso}^{Cu} value is formed predominantly, whereas at higher NO pressures of about 5 Pa, species B is also being formed in higher amounts. Hence it can be inferred that at low NO pressures there is a preference for NO to adsorb at Cu(I) cations, which are coordinated to three oxygen atoms from the framework (species A), whereas at higher NO pressures complex formation at Cu(I) cations coordinated to two framework oxygen atoms also occurs. The presence of two distinct Cu(I)−NO species with different preferences toward NO adsorption was also observed through IR studies by Frache et al.[7] in overexchanged Cu−MCM-22 and is in line with our EPR results. Noticeable differences between overexchanged Cu−MCM-22 and moderately ion exchanged materials occur for the Cu(II) cations. Formation of Cu(II)−NO at 77 K has been reported in the case of overexchanged Cu−MCM-22.[7] The Cu(II) EPR signal intensity is not affected by the adsorbed NO molecules in our case. Thus we must conclude that NO is just adsorbed at Cu(II) species occurring in excess to the nominally ion exchanged cations.

The Cu(II) EPR spectra of Cu−MCM-22 reveal another peculiarity in comparison with the Cu−ZSM-5 system. Although the Cu(II) EPR signal intensity was not affected by NO adsorption in both materials, unlike Cu−ZSM-5, no additional g and A strain effects in the Cu(II) EPR spectra due to NO molecules in the vicinity of the cations could be observed for high NO loadings in the case of Cu−MCM-22 (Figure 7b). This suggests that the Cu(II) ions that are left after dehydration are located at sites in the MCM-22 structure, whose environment is not accessible for NO.

5. Conclusions

Cu(I)−NO complexes were formed over Cu−ZSM-5 and Cu−MCM-22 zeolites, and two different species of Cu(I)−NO complexes could be identified in both systems with similar spin Hamiltonian parameters. The relation $g_{zz} < g_e < g_{xx/yy}$ indicates the presence of Cu 3d orbital contributions to the SOMO of the Cu(I)−NO complex. The large isotropic Cu hf coupling shows that the structure of the complex is bent in both systems, which allows the effective admixture of the 4s orbital of Cu(I) to the SOMO of the Cu(I)−NO moieties. The zeolite matrix does not seem to influence the spin Hamiltonian parameters significantly. It can be concluded that the two different Cu(I)−NO species arise because of the formation of the NO adsorption complexes from Cu(I) at two different sites in the zeolite framework, where it coordinates with either exactly two or two to three oxygens which result in different isotropic Cu hf couplings. In the case of ZSM-5 zeolites, complex formation at the I2 and M7 cation sites could be confirmed by comparison of the experimentally obtained isotropic Cu hf couplings with values predicted by DFT calculations for these sites. We conclude further that similar Cu(I) cation sites must exist in zeolite Cu−MCM-22. The EPR signal intensity decreases at higher NO pressure due to the formation of diamagnetic Cu(I)−$(NO)_2$ dimers. However, dimer formation is completed at distinctly different NO loadings in the two high siliceous zeolites. NO is not found to form adsorption complexes with Cu(II) cations remaining after autoreduction, and the Cu(II) concentration is essentially independent of the NO loading at low temperatures.

Acknowledgment. Financial support of this work by Deutsche Forschungsgemeinschaft (DFG) in the framework of SPP1051 and by the Fonds der Chemischen Industrie is gratefully acknowledged. We are also thankful to Prof. H. Krautscheid, Dipl.-Ing. Joachim Hoentsch, and Dr. Marlen Gutjahr, University of Leipzig, for their help.

Supporting Information Available: Figure S1 showing Q-band EPR spectra of Cu(I)−NO complexes. This material is available free of charge via the Internet at http://pubs.acs.org.

References and Notes

(1) Li, Y.; Hall, W. K. *J. Phys. Chem.* **1990**, *94*, 6145.
(2) Iwamoto, M.; Yashiro H.; Mizuno N. *Nippon Kagaku Kaishi* **1991**, 574. Iwamoto, M. In *Future Opportunities in Catalytic and Separation Technology*; Misono, M., Moro-oks, Y., Kimura, S., Eds.; Elsevier: Amsterdam, 1990.
(3) Sato, S.; Yu-u, Y.; Yahiro, H.; Mizuno, N.; Iwamoto, M. *Appl. Catal.* **1991**, *70*, 11.
(4) Iwamoto, M.; Hamada, H. *Catal. Today* **1991**, *10*, 57.
(5) Iwamoto, M.; Yokoo, S.; Sakai, K.; Kagawa, S. *J. Chem. Soc., Faraday Trans. 1* **1981**, *77*, 1629.
(6) Park, S. K.; Kurshev, V.; Luan, Z.; Lee, C. W.; Kevan, L. *Microporous Mesoporous Mater.* **2000**, *38*, 255.
(7) Frache, A.; Cadoni, M.; Bisio, C.; Marchese, L. *Langmuir* **2002**, *18*, 6875.
(8) Valyon, J.; Hall, K. *J. Phys. Chem.* **1993**, *97*, 1204.
(9) Giamello, E.; Murphy, D.; Magnacca, G.; Morterra, C.; Shioya, Y.; Nomura, T.; Anpo, M. *J. Catal.* **1992**, *136*, 510.
(10) Chao, C. C.; Lundsford, J. H. *J. Phys. Chem.* **1972**, *76*, 1546.
(11) Chao, C. C.; Lundsford, J. H. *J. Am. Chem. Soc.* **1971**, *93* (25), 6794.
(12) Yu, J. S.; Kevan, L. *J. Phys. Chem.* **1994**, *98*, 12436.
(13) Wichterlova, B.; Dedecek, J.; Sobalik, Z.; Vondrova, A.; Klier, K. *J. Catal.* **1997**, *169*, 194.
(14) Cheung, T.; Bhargava, S. K.; Hobday, M.; Foger, K. *J. Catal.* **1996**, *158*, 301.
(15) Sojka, Z.; Che, M., Giamello, E. *J. Phys. Chem.* **1997**, *101*, 4831.
(16) Pöppl, A.; Hartmann, M. *Stud. Surf. Sci. Catal.* **2002**, *142*, 375.
(17) Spoto, G.; Bordiga, S.; Scarno, D.; Zecchina, A. *Catal. Lett.* **1992**, *13*, 39.
(18) Prestipino, C.; Berlier, G.; Llabres i Xamena, F. X.; Spoto, G.; Bordiga, S.; Zecchina, A.; Turnes Palomino, G.; Yamamoto, T.; Lamberti, C. *Chem. Phys. Lett.* **2002**, *363*, 389.
(19) Oka, H.; Okada, T.; Hori, K. *J. Mol. Catal. A* **1996**, *109*, 51.
(20) Dedecek, J.; Sobalik, Z.; Tvaruzkova, Z.; Kaucky, D.; Wichterlova, B. *J. Phys. Chem.* **1995**, *99*, 16327.
(21) Llabres i Xamena, F. X.; Fisicaro, P.; Berlier, G.; Zecchina, A.; Turnes Palomino, G.; Prestipino, C.; Bordiga, S.; Giamello, E.; Lamberti, C. *J. Phys. Chem. B* **2003**, *107*, 7036.
(22) Larsen, S. C.; Aylor, A.; Bell, A. T.; Reimer, J. A. *J. Phys. Chem.* **1994**, *98*, 11533.
(23) Broclawik, E.; Datka, J.; Gil, B.; Kozyra, P. *Phys. Chem. Chem. Phys.* **2000**, *2*, 401.
(24) Lamberti, C.; Bordiga, S.; Salvalaggio, M.; Spoto, G.; Zecchina, A.; Geobaldo, F.; Vlaic, G.; Bellatreccia, M. *J. Phys. Chem. B* **1997**, *101*, 344.
(25) Olson, D. H.; Kokotailo, G. T.; Lawton, S. L. *J. Phys. Chem.* **1981**, *85*, 223.
(26) Nachtigallova, D.; Nachtigall, P.; Sauer, P. J. *Phys. Chem. Chem. Phys.* **2001**, *3*, 1552. Nachtigallova, D.; Nachtigall, P.; Sierka, M.; Sauer, P. J. *Phys. Chem. Chem. Phys.* **1999**, *1*, 2019.
(27) Pietrzyk, P.; Piskorz, W.; Sojka, Z.; Broclawik, E. *J. Phys. Chem. B* **2003**, *107*, 6105.
(28) Lawton, S. L.; Leonowicz, M. E.; Patridge, R. D.; Chu, P.; Rubin, M. K. *Microporpous Mesoporous Mater.* **1998**, *23*, 109.
(29) Wasowicz, T.; Prakash, A. M.; Kevan, L. *Microporous Mater.* **1997**, *12*, 107.
(30) Umamaheswari, V.; Pöppl, A.; Hartmann, M. *J. Mol. Catal. A: Chem.* **2004**, *223*, 123.
(31) Ernst, S. Ph.D. Thesis, University of Karlsruhe, 1987.
(32) Unverricht, S.; Hunger, M.; Ernst, S.; Karge, H. G.; Weitkamp, J. *Stud. Surf. Sci. Catal.* **1994**, *84A*, 37.
(33) Rudolf, T.; Pöppl, A.; Hofbauer, W.; Michel, D. *Phys. Chem. Chem. Phys.* **2001**, *3*, 2167.
(34) Kasai, P. H.; Bishop, R. J., Jr. In *Zeolite Chemistry and Catalysis*; Rabo, J. A., Ed.; ACS Monograph 171; American Chemical Society: Washington, DC, 1976; p 350.
(35) (a) Lunsford, J. H. *J. Chem. Phys.* **1967**, *46*, 4347. (b) Lundsford, J. H. *J. Phys. Chem.* **1968**, *72*, 2141.
(36) Yahiro, H.; Lund, A.; Aasa, R.; Benetis, N. P.; Shiotani, M. *J. Phys. Chem. A* **2000**, *104*, 7950.
(37) Stoll, S. Spectral simulations in solid-state EPR. Ph.D. Thesis, ETH Zurich, 2003.
(38) Gardner, C. L.; Weinberger, W. A. *Can. J. Chem.* **1970**, *48*, 1317.
(39) James, T. C.; Thibault, R. J. *J. Chem. Phys.* **1964**, *41*, 2806.
(40) Pöppl, A.; Rudolf, T.; Manikandan, P.; Goldfarb, D. *J. Am. Chem. Soc.* **2000**, *122*, 10194.
(41) Neyman, K. M.; Ganyushin, D. I.; Nasluzov, V. A.; Rösch, N.; Pöppl, A.; Hartmann, M. *Phys. Chem. Chem. Phys.* **2003**, *5*, 2429.
(42) Freysoldt, C.; Pöppl, A.; Reinhold, J. *J. Phys. Chem. A* **2004**, *108*, 1582.
(43) Ramprasad, R.; Hass, K. C.; Schneider, W. F.; Adams, J. B. *J. Phys. Chem. B* **1997**, *101*, 6903.
(44) Davidova, M.; Nachtigallova, D.; Nachtigall, P.; Sauer, J. *J. Phys. Chem. B* **2004**, *108*, 13674.